Spatiotemporal compartmentalization of key physiological processes during muscle precursor differentiation

Ertuğrul M Özbudak[a,b], Olivier Tassy[a,c], and Olivier Pourquié[a,c,d,e,f,g,h,1]

[a]Stowers Institute for Medical Research, Kansas City, MO 64110; [b]Department of Genetics, Albert Einstein College of Medicine, Bronx, NY 10461; [c]The Howard Hughes Medical Institute, Kansas City, MO 64110; [d]University of Kansas Medical Center, Kansas City, KS 66160; [e]Institut de Génétique et de Biologie Moléculaire et Cellulaire; [f]Institut National de la Santé et de la Recherche Médicale, U.964, and [g]Centre National de la Recherche Scientifique, UMR7104, Illkirch, F-67400 France; and [h]Université de Strasbourg, Strasbourg, F-67000 France

Edited by Steven L. McKnight, University of Texas Southwestern, Dallas, TX, and approved January 13, 2010 (received for review August 20, 2009)

The development of multicellular organisms is controlled by transcriptional networks. Understanding the role of these networks requires a full understanding of transcriptome regulation during embryogenesis. Several microarray studies have characterized the temporal evolution of the transcriptome during development in different organisms [Wang QT, et al. (2004) *Dev Cell* 6:133–144; Furlong EE, Andersen EC, Null B, White KP, Scott MP (2001) *Science* 293:1629–1633; Mitiku N, Baker JC (2007) *Dev Cell* 13:897–907]. In all cases, however, experiments were performed on whole embryos, thus averaging gene expression among many different tissues. Here, we took advantage of the local synchrony of the differentiation process in the paraxial mesoderm. This approach provides a unique opportunity to study the systems-level properties of muscle differentiation. Using high-resolution, spatiotemporal profiling of the early stages of muscle development in the zebrafish embryo, we identified a major reorganization of the transcriptome taking place in the presomitic mesoderm. We further show that the differentiation process is associated with a striking modular compartmentalization of the transcription of essential components of cellular physiological programs. Particularly, we identify a tight segregation of cell cycle/DNA metabolic processes and translation/oxidative metabolism at the tissue level, highly reminiscent of the yeast metabolic cycle. These results should expand more investigations into the developmental control of metabolism.

mesoderm | metabolism | stem cell | transcription factors

The vertebrate body forms by the progressive elongation of the embryonic axis at its posterior end. This process resembles the polarized growth from a terminal meristem observed in plants (1). It results in the progressive deposition of new cells from a terminal growth zone (the tail bud), hence, generating a flux of derivatives of the three germ layers. These newly produced cells begin to differentiate when they exit the posterior growth zone. Thus, an important consequence of this process is that cells located at a more posterior position along the antero-posterior (AP) axis are in a more immature state than cells located more anteriorly in the embryo. Therefore, during the axis elongation phase, the AP axis of the embryo corresponds to a projection of the temporal differentiation of cells of the body axis. The paraxial mesoderm is a major component of the embryonic axis that forms the presomitic mesoderm (PSM) posteriorly and the segmented somites anteriorly (Fig. 1*A*). Somites contain the precursors of skeletal muscles, vertebrae, and dorsal dermis. Thus, along the AP axis, the paraxial mesoderm exhibits progressively more mature differentiation stages (Fig. 1*A*). Furthermore, unlike other tissues (e.g., the neural tube, where differentiation proceeds heterogeneously), cells in the PSM are locally synchronized with each other with respect to their differentiation and gene expression.

Here, we took advantage of these two striking properties to analyze paraxial mesoderm differentiation using high-resolution, temporal microarray profiling. We focused on microdissected pieces derived from tissue isolated from single embryos, which avoids averaging gene expression among different cell types as compared with earlier transcriptome studies (2–5). Our results revealed temporal compartmentalization of metabolic processes as the precursors of muscle cells commit to differentiate.

Results

High-Resolution Spatial Profiling of Gene Expression Along the PSM Reveals the Temporal Trajectory of Transcriptome Changes as Cells Commit to Differentiate. We dissected the posterior end of the paraxial mesoderm—including the PSM and the recently formed somites—from both sides of 12-somite zebrafish embryos (Fig. 1*B*). Subsequently, we divided the tissue from each side into an equivalent number of similar-sized fragments, corresponding to roughly the size of two somites. Then, these fragments were processed for microarray analysis as described in *Materials and Methods* (6). In this way, we obtained a duplicate series of six samples corresponding to progressively more advanced differentiation stages, ranging from the immature tail-bud stage to the newly formed somite, which in zebrafish mostly corresponds to muscle progenitors (Fig. 1*B*) (7). Because the somitic precursors are linearly arrayed in the PSM, and knowing that production of one somite takes ~30 min in zebrafish, each consecutive sample is spaced by ~60 min. Therefore, this sample set provides a series of snapshots of the evolution of the paraxial mesoderm transcriptome between the tail-bud/epiblast stage and the muscle precursor stage at a 60-min resolution. The total series corresponds to ~6 h of differentiation. The results from microarrays generated from fragments originating from the same level of the left and the right sides for each spatial point along the PSM were compared with each other and found to be highly correlated, confirming the quality of the microarray samples (Table S1). We aligned microarray data from the different spatial domains along this temporal trajectory to compare gene expression between cells located at different spatial positions and to reveal the temporal trajectory of transcriptome changes along the body axis as cells commit to differentiate to the muscle lineage.

We first examined a sample of more than 50 genes known to be expressed nonubiquitously along the axis, based on the literature, and observed that they are accurately detected in our dataset in the correct spatial regions. This list includes genes expressed in a posterior-to-anterior gradient along the AP axis;, for example: (*i*) the Fgf and Wnt targets *Mesogenin1* or *Brachyury* (8), (*ii*) genes expressed

Author contributions: E.M.O. and O.P. designed research; E.M.O. performed research; E.M.O., O.T., and O.P. analyzed data; and E.M.O., O.T., and O.P. wrote the paper.

The authors declare no conflict of interest.

This article is a PNAS Direct Submission.

[1]To whom correspondence should be addressed. E-mail: pourquie@igbmc.fr.

This article contains supporting information online at www.pnas.org/cgi/content/full/0909375107/DCSupplemental.

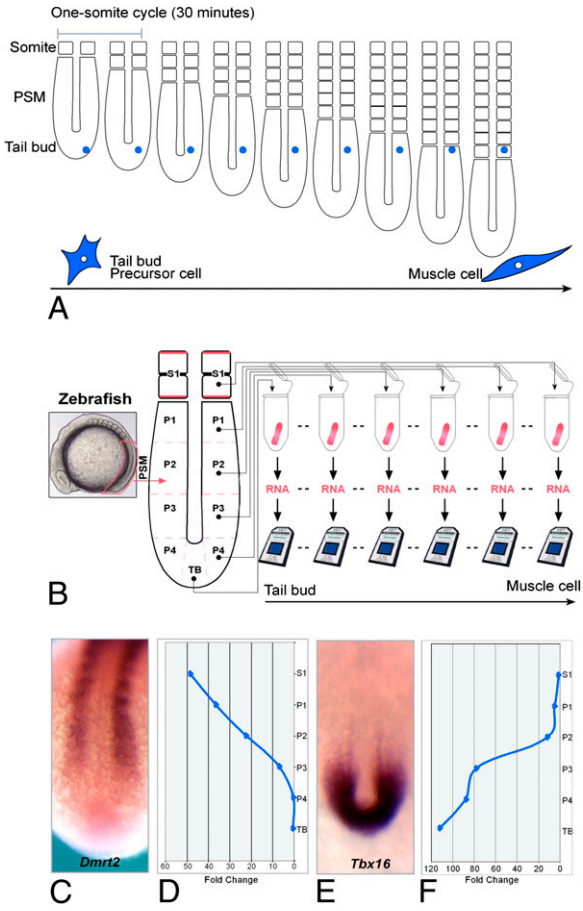

Fig. 1. Generation of a microarray time series covering early stages of muscle differentiation in the zebrafish embryo. (*A*) A descendent of the tail-bud precursor cells (blue cell) enters the PSM posteriorly and progressively matures as it become located more and more anteriorly in the PSM during axis elongation. The cell eventually becomes incorporated into a somite, where most cells differentiate into muscles in zebrafish embryos. (*B*) Generation of the microarray time series. (*Left*) Lateral view of a 12-somite zebrafish embryo showing the position of the PSM (pink box). The samples used for the microarray time series were collected from six consecutive spatial positions in the PSM and recently formed somites on both sides of an embryo. Microarray expression profiles (*D* and *F*) faithfully recapitulate the expression of *Dmrt2* (*C*) and *Tbx16* (*E*) detected by in situ expression in 15-somite zebrafish embryos. Expression levels (*D* and *F*) were normalized by the expression levels in the tail bud (TB) and the somites (S1), respectively, to show the fold increase or decrease, respectively, along the spatial axis.

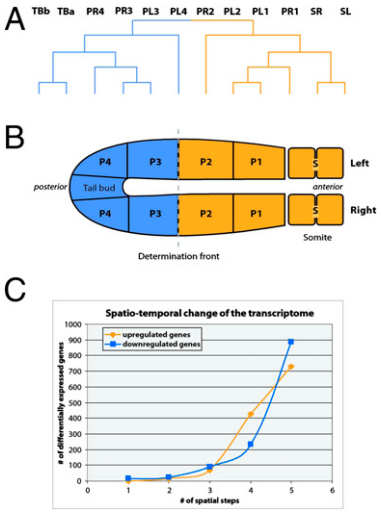

Fig. 2. Hierarchical clustering identifies a major subdivision of the PSM. (*A*) Unsupervised HCL clustering of the 12 array samples by Spearman Rank Correlation metric with average linkage clustering. (*B*) Blue and orange illustrate the grouping that maximizes the number of differentially expressed genes obtained by SAM analysis. The identified division corresponds to the same division obtained by HCL in *A*. (*A* and *B*) L and R, left and right samples, respectively; P1, anterior PSM; P2, intermediate PSM; P3, posterior PSM; P4, tail region flanking the tail bud; S, formed somite. Group 1 represents the posterior samples (blue) and group 2 represents the anterior samples (orange). (*C*) Total number of differentially expressed genes as cells moves from the tail bud to the formed somites. Numbers were obtained using 10% FDR with SAM analysis and more than a 1.5-fold change in expression levels.

with a graded pattern in an opposite orientation, *Dmrt2/Terra* (9), and (*iii*) genes showing local expression domains and stripes in the PSM, including *mesp-a* and *-b* genes (10) (Fig. 1 *C–F* and Fig. S1).

Clustering of Spatial Samples Points to a Major Transcriptome Reorganization at the Determination Front Level. We next examined quantitative changes in the transcriptome and characterized how quickly these changes occur as cells travel along the differentiation axis. To address these questions, we first used a hierarchical clustering (HCL) method (11) to evaluate the similarity among the different samples. Closely spaced samples were generally observed to cluster together (Fig. 2*A*). However, the posterior paraxial mesoderm can be divided into two major spatial domains: one composed of formed somites and the anterior and intermediate PSM, the second composed of the posterior PSM and the tail-bud region (Fig. 2*A*). Strikingly, the separation between these two domains roughly corresponds to the determination front, where the segmental prepattern is first established (8). At this level, PSM cells respond to the periodic signal of the segmentation clock by activating expression of the transcription factors of the Mesp family in a striped domain. These stripes provide the blueprint used to form the future somite.

We then divided the 12 samples into all possible combinations of two groups using the Significance Analysis of Microarrays (SAM) algorithm (12) to identify differentially expressed genes between the groups in each combination. We reasoned that groupings that maximize the number of differentially expressed genes should correspond to biological divisions of the tissue. Strikingly, this strategy also identified the determination front as marking a sharp divide, suggesting that it reflects a major functional division in the tissue (Fig. 2*B*) (8).

Gene Ontology Statistics of Genes Differentially Expressed Along the Axis Unraveled a Metabolic Switch During Commitment to Differentiation. We next identified the genes that change their expression levels along this differentiation axis. We used SAM to compare the expression levels of genes in cells in the most immature (tail bud) stage (i.e., the ground state) to that of progressively more mature levels. The total number of differentially expressed genes clearly indicates an exponential-like increase, from the point cells enter the tissue to the point they exit the PSM. In total, 733 genes are up-regulated, of which 132 are activated de novo in the anterior PSM and 889 are down-regulated out of ~6,000 genes detected in the fish paraxial mesoderm [with 10% false-discovery rate (FDR) and 1.5-fold change in gene expression] (Fig. 2*C*). Thus, the transcriptional landscape of cells from the tail bud remains essentially unchanged until they reach the determination front, where a major reorganization of the expressed transcriptome occurs soon after segmental determination in the PSM.

We developed a database called Manteia to improve the zebrafish microarray annotation by linking the fish Affymetrix probesets to

corresponding National Center for Biotechnology Information or ENSEMBL zebrafish gene models and merging the available information for both. Manteia also offers the possibility to enhance this annotation by inferring to the fish gene models the annotation [such as Gene Ontology (GO) terms] of their corresponding human and mouse orthologs. The database provides convenient statistical tools to evaluate the enrichment of GO categories compared to the genome or to the transcriptome represented on the microarray. Thus, we analyzed the enrichment in specific GO categories for the genes whose levels are changing along the differentiation axis (Dataset S1). We observed a strikingly simple landscape of enriched categories for the genes that are down and up-regulated during differentiation (Fig. 3*A* and Dataset S1). For the down-regulated genes, the enriched functions include: development (281 genes), signaling (62 genes), NADP and amino acid metabolism (22 genes), transcription (194 genes), nuclear import and protein metabolism (228 genes), and cell cycle/DNA metabolism (184 genes) (Dataset S1). As expected, the signaling GO categories include terms linked to Wnt and FGF pathways, which show graded signaling along the PSM (8). Interestingly, this analysis also identified the Rho pathway as a prominent signaling pathway in the posterior PSM. In the development category, a very significant enrichment in terms related to mesoderm and ectoderm development is identified but, strikingly, only one GO term related to endoderm development is observed. A prominent function identified in the down-regulated genes corresponds to cell-cycle/DNA metabolism. It includes GO terms such as "replication, mitosis" and "DNA repair" (Dataset S1). Transcription is represented as a major class of GO terms and includes mostly transcription factors and proteins involved in the transcription machinery. Terms related to nuclear import and protein metabolism (e.g., proteases, ubiquitin pathway) are also highly enriched. The terms related to metabolism show very striking specificity because they essentially belong to the glutamine biosynthetic pathway, as well as to the NADP metabolic process, which in fact is essentially the pentose-phosphate pathway (Fig. 3*C*).

Signaling (6 genes), development (139 genes), and transcription (149 genes) classes are also identified in the up-regulated genes but contain very different terms (Dataset S1). For example, the signaling category contains only the Notch signaling pathway term and the development and transcription categories contain fewer different terms and genes identified than for the down-regulated genes. Another smaller category we identified contains terms related to adhesion and motility (30 genes). The major function identified in up-regulated GO categories during differentiation relates to translation and oxidative metabolism (334 genes). This group includes all of the functions related to protein translation and oxidative metabolism (e.g., tRNA metabolism, RNA processing, ribosome biogenesis, respiratory function, Adenosine-5′-triphosphate [ATP] production, mitochondrial organization, and translation initiation and elongation) (Fig. 3*A*, Table S2, and Dataset S1). A significant number of genes functioning at different steps of the respiratory chain are identified as up-regulated in the somites (Table S2). Up-regulated genes involved in protein synthesis include 48 ribosomal proteins, 13 RNA processing proteins, 12 translation initiation and 3 elongation factors, and 5 proteins involved in protein folding. Thus, in these processes, not only limiting steps but also a large portion of the machinery appears to be up-regulated in paraxial mesoderm differentiation.

We then used the short time-series expression miner (STEM) program (13) to identify the major expression patterns represented in the paraxial mesoderm differentiation time series. Using this algorithm, we identified a number of significant patterns in the array series (Fig. 3*B*). The two largest categories of patterns each include four profiles and correspond to up-regulated genes (Fig. 3*B*, green; 828 genes) and down-regulated genes (Fig. 3*B*, pink; 709 genes). The third category includes genes (Fig. 3*B*, yellow; 136 genes) whose expression peaks in the middle of the series. We then examined the GO categories enriched for all of these profiles. This analysis identified classes of GO categories that are essentially similar to the ones identified for the up- and down-regulated genes by SAM (Dataset S1) and confirmed the enrichment in cell cycle/DNA metabolic functions in the posterior PSM and in translation/oxidative metabolism in the anterior PSM and somites. The STEM analysis also increased the resolution and allowed identification of more functions compartmentalized in time during differentiation.

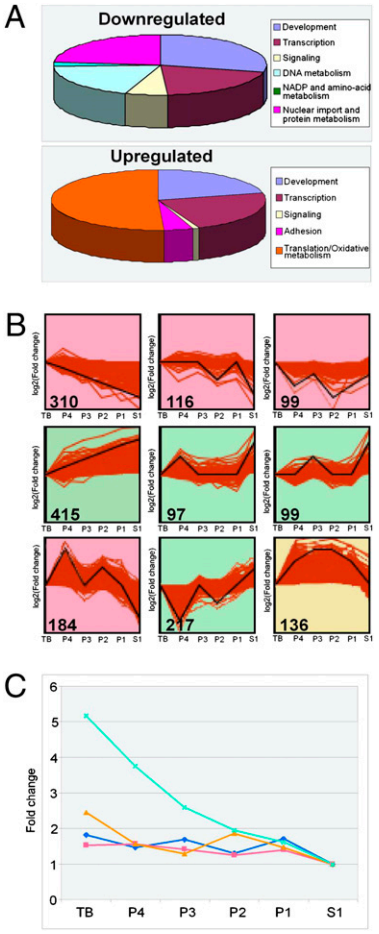

Fig. 3. Significant biological functions and gene-expression patterns identified during the differentiation of paraxial mesoderm cells. (*A*) Pie charts illustrating the GO categories statistically enriched (less than 10% FDR and 1.5-fold change in expression) in the down-regulated genes (*Upper*) or up-regulated genes (*Lower*). The number of spatially down-regulated genes associated with the "Development," "Transcription," "Signaling," "DNA metabolism," "NADP and amino-acid metabolism," and "Nuclear import and protein metabolism" GO terms are 281, 194, 62, 184, 22, 228, respectively. The number of spatially up-regulated genes associated with the "Development," "Transcription," "Signaling," "Adhesion," "Translation/Oxidative Metabolism" GO terms are, respectively, 139, 149, 6, 30, 334. (*B*) Significant profiles (<5% Bonferroni correction method) detected out of 50 profiles using STEM analysis. The number of genes belonging to each profile is shown in each frame (e.g., 310, 116, 99). Red curves represent individual probeset profiles; the black line represents the profile to which probesets are most similar. Genes are either down-regulated (pink), up-regulated (green), or peaking in the middle (yellow). *y* axis represents $\log_2$ (fold-change) of expression values along the axis. Fold-change is measured by normalizing the expression values to those in the tail bud (i.e., left-most value in the graphs are equal to 1). On the *x* axis are the spatial points starting from tail bud (*Left-most*) ending at the somites (*Right-most*). The minimal variation step between two points in the graph represents a 2-fold change in the expression values. Larger steps correspond to a 4-fold change. (*C*) Expression profiles of four down-regulated genes—*pgd* (green), two *Hibadh* paraloges (yellow hibadha and dark blue hibadhb), and *taldo1* (pink)—that belong to the GO term NADP metabolic process. Profiles normalized to the expression levels in the somites (S1); *P*, presomitic mesoderm; TB, tail bud.

For example, the cluster showing a peak in the middle of the series is highly enriched in terms related to actin cytoskeleton and cell motility (Fig. 3*B*, yellow, and Dataset S1). In addition, one of the up-regulated clusters that shows a peak of expression in the middle of the series was selectively enriched in terms related to vesicle biogenesis (Dataset S1). Thus, this analysis demonstrates that the major gene-expression patterns detected in the PSM essentially correspond to those of the up- or down-regulated genes detected in our SAM analysis.

Biological Evidence for Spatial Compartmentalization of DNA Metabolism and Respiration in the Paraxial Mesoderm. We then attempted to validate whether the enrichment in these GO categories translates into corresponding biological functions in vivo. We first evaluated the regulation of cell cycle/DNA metabolism by analyzing the DNA content of PSM cells at different differentiation stages by measuring incorporation of the fluorescent dye propidium iodide (Fig. 4*A*). Sections of zebrafish embryos, including either the posterior PSM and tail bud or the last five formed somites, were pooled from different embryos and dissociated into single cells. These cells were then labeled with propidium iodide and analyzed by flow cytometry. The results indicate that the average DNA content per cell is higher in the posterior region of the embryo, supporting the idea that DNA synthesis and cell proliferation are enriched posteriorly in comparison with the formed somites. This result is consistent with the observed reduction in the expression of genes belonging to cell cycle/DNA metabolism as cells travel along the axis.

We then focused on the evolution of the transcriptional landscape during differentiation and compared the number of transcription factors that are present in the tail bud to those expressed in the formed somites. Our analysis indicates that only the genes down-regulated along the axis are enriched with the GO category "regulation of transcription, DNA dependent." Based on the GO term "transcriptional regulatory activity," a total of 447 genes were found to be expressed at different levels in the tail-bud region (Dataset S1). Of these genes, 105 were significantly down-regulated, and 42 were up-regulated in the somites (Dataset S1). In addition, 29 new transcription factors were activated de novo in the formed somites. This analysis identified the majority of the expected transcription factors associated with PSM and somite maturation, including TBX24, paraxis, and DMRT2/Terra (14–16), as well as with muscle precursor specification such as myf5, Myogenin1, Six4, and Eya1 (7). Interestingly, other transcription factors involved in Myogenesis, including Foxk1 (17), Tcf12/HEFb (18), and Fox05/Fox03 (19) were also identified in this list. The transcription factor MycA, which is involved in the control of growth in many systems (20), is up-regulated in the anterior PSM and, thus, could play a role in the control of the up-regulation of the translation/respiration function. Therefore, during their maturation process, the more immature tail-bud cells down-regulate more transcription factors than they up-regulate. Whereas stem cells or immature precursors are often considered as naïve cells, this finding suggests that the transcriptional repertoire of the tail-bud cells is actually more complex than that of differentiated cells.

We next verified the increase in the expression of genes belonging to the GO categories translation, mitochondrion organization and biogenesis, ribonucleoprotein complex biogenesis, and assembly and RNA processing by performing qPCR for selected genes. Thirty out of 41 genes tested increased more than 20%, whereas the other 11 were either increased or decreased less than 1.2 fold (Dataset S1 and Table S3). To validate whether the observed changes in gene expression resulted in functional changes in biological processes, we measured the ratio of ATP and total protein levels (normalized to DNA levels) in the anterior-vs.-posterior sections of the axis (Fig. 4*B*). An increase of ~2-fold in both ATP and total protein levels was observed between the posterior PSM and the formed somites (Fig. 4*B*). To further

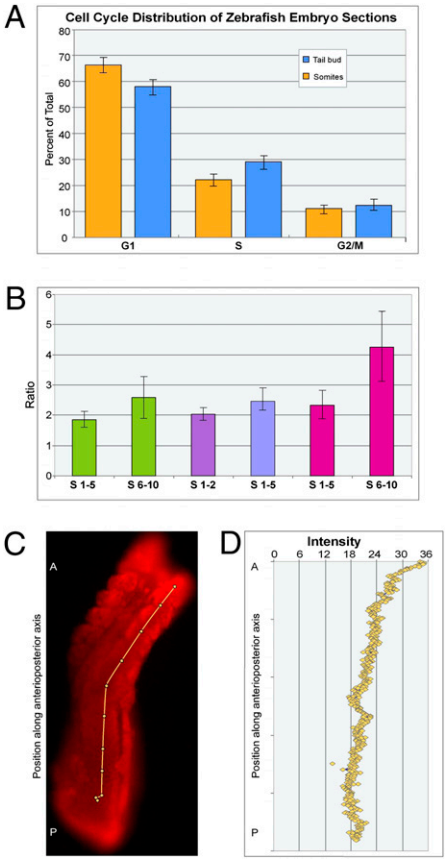

Fig. 4. Biological validation of the compartmentalization of cell cycle/DNA metabolism and translation/oxidative metabolism along the PSM. (*A*) The DNA content of tail bud cells (orange) is compared against the last six-to-eight formed somites (blue) from both the *Left* and *Right* sides. *P* values from the one-tail *t* test are 0.00019, 0.00043, and 0.0589 for the three phases, respectively. Standard deviations are plotted in the panel. (*B*) The ratio of different measurements (values are obtained from cells in the anterior locations and divided by those in the posterior locations) are shown in histograms. The total protein level (green) is increased in the anterior sections of the embryo 1.8-fold and 2.5-fold, at the spatial position: somites 1 to 5 (S 1–5) or somites 6 to 10 (S 6–10), respectively, compared with that of the posterior PSM. The ATP level (purple) is increased 2-fold in somites 1 and 2 (S 1–2) compared with the tail bud. The cytochrome-C oxidase activity level (blue) is also increased in the last five formed somites (S 1–5) by 2.5-fold compared with the posterior PSM. H_2O_2 level (pink) also progressively increases in the anterior sections of the embryo from 2.3-fold and 4.3-fold, at spatial position: somites 1 to 5 (S 1–5) or somites 6 to 10 (S 6–10), respectively, compared with that of in the posterior PSM. All ratios were obtained by normalizing by DNA content in the respective samples. Error bars represent SEM. (*C*) A representative zebrafish embryo stained with MitoTracker Orange CM-H_2TMROS. (*D*) *y* axis shows the intensity of fluorescence measured along the anterioposterior axis through the yellow line in *C* from somites (A, anterior) to the tail bud (*P*, posterior).

examine whether the change in ATP levels is linked to changes in mitochondrial activity, we first used the MitoTracker Orange CM-H_2TMROS dye, which only fluoresces when it enters an actively respiring cell, where it becomes oxidized. Analysis of the fluorescence profile of intact embryos (n = 6) labeled with MitoTracker showed an overall 2-fold increase in the level of fluorescence as cells become located at more anteriorly along the axis (Figs. 4 *C* and *D*). To examine changes in the respiratory activity of the cells during differentiation, we also measured the Cytochrome-C Oxidase levels in the last five formed somites and compared them to the levels in the tail bud. The ratio indicates that Cytochrome-C Oxidase activity is 2.5-fold increased in the anterior segments (Fig. 4*B*). The increased oxidative metabolism and

DEVELOPMENTAL BIOLOGY

mitochondrial function observed in more differentiated cells is expected to lead to an increase in the levels of reactive oxygen species and hydrogen peroxide (H_2O_2) byproducts. To verify this, we used a Horseradish peroxidase-based assay to detect H_2O_2 levels. We observed a substantial increase in the H_2O_2 levels in the differentiating cells compared with the progenitor cells (Fig. 4*B*). Together, our results demonstrate a striking compartmentalization between cell cycle/DNA metabolism and translation/respiration along the paraxial mesoderm.

Discussion

When yeast cells are exposed to constant but limiting amounts of nutrients, they begin to implement a complex 5-h metabolic cycle involving periodic transcriptional regulation of most major metabolic functions (21). This cycle is characterized by their alternating between a reductive phase gating of the cell cycle and an oxidative/respiratory phase devoted to energy production and translation. The segregation of the cell cycle from the respiratory phase is critical to protect it from DNA damage arising from the byproducts of respiration (22). The striking spatiotemporal compartmentalization of functions related to cell-cycle/DNA metabolism and translation/oxidative metabolism along the PSM is highly reminiscent of that described for the yeast metabolic cycle (YMC) and might also serve to protect stem cells in the highly proliferative areas of the embryo from potential damage resulting from the active oxidative metabolism required for growth. Similarity between the YMC and the cell-differentiation sequence in the PSM further extended beyond the broad cell cycle and growth functions. For example, in yeast the reductive phase is associated with an increase in endocytic processes, resulting in the building of the vacuole during the reductive phase of the cycle (21). Similarly, in the PSM, our STEM analysis detected a transient up-regulation of genes involved in vesicle-mediated transport (Fig. 3*B* and Dataset S1). Another striking function conserved between the two systems includes the pentose-phosphate pathway (23). This pathway plays a major role in the production of NADPH (a reduced form of NADP+), a key metabolite that provides the cell with reductive power, and which is involved in the production of intermediates for many biosynthetic reactions. During differentiation, we observed a strong down-regulation of key enzymes of the pentose-phosphate pathway, such as phosphogluconate dehydrogenase, which generates NADPH, and transaldolase 1 both of which are involved in converting sugar intermediates back to 5-carbon sugar that can be used for glycolysis (Fig. 3*C*). Other enzymes, such as the 3-hydroxyisobutyrate dehydrogenase, which is involved in the production of NADH, were also regulated in a similar fashion (Fig. 3*C*). These results are consistent with an active production of reductive agents (e.g., NADPH/NADH) in the posterior part of the PSM, further emphasizing its similarity with the YMC reductive phase.

Spatiotemporal compartmentalization of metabolic processes has been reported in various organisms, ranging from cyanobacteria and yeast to animals (24–26). In vertebrates, functions, such as the cell cycle or energy production, are also under temporal circadian regulation and are differentially regulated depending on the organ considered (27). Therefore, our data suggest that the logics of the temporal compartmentalization of metabolic reactions could represent a basic property of metabolic regulation in living cells.

Materials and Methods

Sample Preparation. Wild-type embryos from the AB line were grown at 23 °C up to 12-somite-stage and used for the dissections in all of the experiments. Embryos were deyolked manually, the skin removed, and the embryo flattened on a surface similar to that as described previously (28), with the exception that during the dissections, AMP-PNP was not applied to the embryos to avoid any side effects. The PSM from each side of the axial tissues was dissected from the rest of the embryo and divided into five different domains. The left and right sides of the PSM were dissected separately. Because there is only one tail-bud domain and its size is limited, a second sample of the same region was obtained from a second stage-matched embryo. The last two somites formed from a third stage-matched embryo (both right and left sides) were added as the sixth anterior-most piece along the axis. The isolated fragments were placed in TRIzol solution (Invitrogen) and frozen immediately at −80 °C. Total RNA was isolated from these fragments.

RNA Preparation and Microarray Analysis. Total RNA extracted from the dissected fragments (~400 cells) was amplified by using Affymetrix GeneChip Expression 3′Amplification two-Cycle cRNA Snythesis Kit. Biotinylated cRNA were prepared by using Affymetrix GeneChip Expression 3′-Amplification Reagents for IVT Labeling kit. The quantity and the quality of the amplified RNA were assessed by spectrometry and bioanalyzer, respectively. Amplified and fragmented 13 μg of cRNA was hybridized to the zebrafish Affymetrix chips. Arrays were hybridized according to the manufacturer's instructions and scanned with an Affymetrix GeneChip Scanner 3000 7G at the Microarray Core Facility of the Stowers Institute for Medical Research. Array output was analyzed by using Affymetrix Microarray Suite 5.0 and scaled by adjusting the average intensity of each array to a target intensity of 150. The array data, including the raw CEL files and the processed/normalized data (Dataset S1), along with experimental descriptions have been deposited in GEO (GEO accession number for the full dataset is GSE15796).

The intensities of the left and right side samples of each spatial point were compared with each other and found to be highly correlated (Table S1), confirming the quality of the microarray samples. As expected, the correlations of the samples from different spatial points decreased linearly with the spatial distance between the samples. The high correlation of the two tail-bud samples and the close-distance clustering of these two samples in the HCL analysis indicate that our method is robust against embryo-to-embryo changes.

HCL Clustering. We filtered out any probeset that was not called "present" in at least two arrays or called "present" in one, but also called "marginal" in two other arrays out of 12 total arrays. The HCL clustering of the spatial samples was performed using the MultiExperiment Viewer Version 4.0 (29). Spearman Rank Correlation metric was used with average linkage clustering.

SAM Analysis. To identify differentially expressed genes, the SAM algorithm (12) from the MultiExperiment Viewer, Version 4.0 (29) was used. The filtered probeset list was used as the input. A two-class unpaired grouping was used, and the Tusher et al. (12) method was selected to calculate S0 parameter. FDR (10%) with 1.5-fold-change was set as the threshold for a probeset to be called differentially detected between the two groups of samples. The lists of differentially expressed genes were obtained using Manteia (*Annotation and Analysis Strategy in Manteia* section in *SI Materials and Methods*). The names of the probesets and corresponding gene descriptions are provided (Dataset S1).

The overlap of the differentially expressed gene data with the literature is very good. The majority of the known genes [>50 expressed nonubiquitously along the axis based on published in situ hybridization images (http://zfin.org/cgi-bin/webdriver?MIval=aa-xpatselect.apg)] (Fig. S1), are detected in our data in the correct spatial regions. This list includes genes belonging to Fgf, Wnt, and RA (retinoic acid) signaling pathways, as well as *T-box*, *mesp*, and *gadd45* genes. Moreover, we performed qPCR for selected genes belonging to GO categories enriched in the last formed somites. The results agree well with microarray data (Table S3) See Table S4 for the sequences of the primer sets.

STEM Analysis. The present probeset list was filtered further to include only the probesets in the top 50% variance. No further filtering was done in STEM (13) based on expression levels (see *SI Materials and Methods* file for the parameter details).

Gene Ontology Enrichment Statistics. GO enrichment statistics were done using Manteia database (see *SI Materials and Methods* for details). Manteia is accessible at http://research.stowers-institute.org:8000/Manteia.

Cell Cycle Analysis. The DNA content of the entire tail bud and the flanking PL4 and PR4 domains were compared with the last six to eight somites formed (including both the left and right sides of the paraxial mesoderm and the axial tissues in between). Each experiment contained samples from at least 12 or 7 embryos from the tail bud and somite sections, respectively, and 12 to 15 somite-stage embryos were dissected. Dissected sections were trypsinized for 5 min and dissociated into single cells using glass needles. Cells were fixed in 70% EtOH overnight at −20 °C. The samples were stained with propidium iodide and cell-cycle distribution was collected on InFlux by Flow cytometry and analyzed by ModFit.

Statistical Analysis. One-tailed *t* test with unequal variance was performed to assess the significance of cell-cycle analysis data. In total, seven experiments for the somites and six experiments for the tail-bud region were conducted. SDs are plotted in Fig. 4*A*.

Measurements of Total Protein Levels. Bio-Rad Protein Assay (Bradford) was used to measure the total protein levels (*SI Materials and Methods*).

Measurements of ATP Levels. ATPlite Luminescence ATP Detection Assay System (Perkin-Elmer) was used to measure the ATP levels (*SI Materials and Methods*).

Measurements of Cytochrome-C Oxidase Activity. Cytochrome-C Oxidase Assay Kit (Sigma) was used to measure the cytochrome-C oxidase activity (*SI Materials and Methods*).

MitoTracker Staining. MitoTracker Orange CM-H_2TMROS (M7511, Molecular Probes-Invitrogen) was used to measure mitochondrial respiratory activity (*SI Materials and Methods*).

Measurements of Hydrogen Peroxide Levels. H_2O_2 levels were measured by using the Amplex Red Hydrogen Peroxide/Peroxidase Assay Kit (Molecular Probes, A22188) (*SI Materials and Methods*).

RT-PCR Measurements. Average fold-change of the expression of a large set of genes in the tail-bud region versus the last two somites are measured (*SI Materials and Methods*).

ACKNOWLEDGMENTS. The authors thank S. Mathur for helpful discussions and help on statistical analysis and members of the Pourquié laboratory for critical reading of the manuscript and discussions; J. Chatfield for editorial assistance and S. Esteban for artwork; the Stowers Institute core facilities, and D. Baumann, J. Wunderlich, and A. Peak. Research was supported by Stowers Institute for Medical Research, and in part by the Defense Advanced Research Projects Agency Grant HR 0011-05-1-0057 (to O.P.). Zebrafish were obtained from the Zebrafish International Resource Center at the University of Oregon, which is supported by a grant from the National Institutes of Health–National Center for Research Resources. This work was funded by the Howard Hughes Medical Institute.

1. Brady SM, et al. (2007) A high-resolution root spatiotemporal map reveals dominant expression patterns. *Science* 318:801–806.
2. Wang QT, et al. (2004) A genome-wide study of gene activity reveals developmental signaling pathways in the preimplantation mouse embryo. *Dev Cell* 6:133–144.
3. Furlong EE, Andersen EC, Null B, White KP, Scott MP (2001) Patterns of gene expression during *Drosophila* mesoderm development. *Science* 293:1629–1633.
4. Mitiku N, Baker JC (2007) Genomic analysis of gastrulation and organogenesis in the mouse. *Dev Cell* 13:897–907.
5. Ouyang M, et al. (2008) A web based resource characterizing the zebrafish developmental profile of over 16,000 transcripts. *Gene Expr Patterns* 8:171–180.
6. Dequéant ML, et al. (2006) A complex oscillating network of signaling genes underlies the mouse segmentation clock. *Science* 314:1595–1598.
7. Bryson-Richardson RJ, Currie PD (2008) The genetics of vertebrate myogenesis. *Nat Rev Genet* 9:632–646.
8. Dequéant ML, Pourquié O (2008) Segmental patterning of the vertebrate embryonic axis. *Nat Rev Genet* 9:370–382.
9. Saúde L, Lourenço R, Gonçalves A, Palmeirim I (2005) *Terra* is a left-right asymmetry gene required for left-right synchronization of the segmentation clock. *Nat Cell Biol* 7:918–920.
10. Sawada A, et al. (2000) Zebrafish Mesp family genes, *mesp-a* and *mesp-b* are segmentally expressed in the presomitic mesoderm, and *Mesp*-b confers the anterior identity to the developing somites. *Development* 127:1691–1702.
11. Eisen MB, Spellman PT, Brown PO, Botstein D (1998) Cluster analysis and display of genome-wide expression patterns. *Proc Natl Acad Sci USA* 95:14863–14868.
12. Tusher VG, Tibshirani R, Chu G (2001) Significance analysis of microarrays applied to the ionizing radiation response. *Proc Natl Acad Sci USA* 98:5116–5121.
13. Ernst J, Bar-Joseph Z (2006) STEM: a tool for the analysis of short time series gene expression data. *BMC Bioinformatics* 7:191.
14. Nikaido M, et al. (2002) Tbx24, encoding a T-box protein, is mutated in the zebrafish somite-segmentation mutant fused somites. *Nat Genet* 31:195–199.
15. Burgess R, Cserjesi P, Ligon KL, Olson EN (1995) Paraxis: a basic helix-loop-helix protein expressed in paraxial mesoderm and developing somites. *Dev Biol* 168: 296–306.
16. Seo KW, et al. (2006) Targeted disruption of the DM domain containing transcription factor Dmrt2 reveals an essential role in somite patterning. *Dev Biol* 290:200–210.
17. Bassel-Duby R, et al. (1994) Myocyte nuclear factor, a novel winged-helix transcription factor under both developmental and neural regulation in striated myocytes. *Mol Cell Biol* 14:4596–4605.
18. Parker MH, Perry RL, Fauteux MC, Berkes CA, Rudnicki MA (2006) MyoD synergizes with the E-protein HEB beta to induce myogenic differentiation. *Mol Cell Biol* 26: 5771–5783.
19. Hu P, Geles KG, Paik JH, DePinho RA, Tjian R (2008) Codependent activators direct myoblast-specific MyoD transcription. *Dev Cell* 15:534–546.
20. Eilers M, Eisenman RN (2008) Myc's broad reach. *Genes Dev* 22:2755–2766.
21. Tu BP, Kudlicki A, Rowicka M, McKnight SL (2005) Logic of the yeast metabolic cycle: temporal compartmentalization of cellular processes. *Science* 310:1152–1158.
22. Chen Z, Odstrcil EA, Tu BP, McKnight SL (2007) Restriction of DNA replication to the reductive phase of the metabolic cycle protects genome integrity. *Science* 316: 1916–1919.
23. Tu BP, et al. (2007) Cyclic changes in metabolic state during the life of a yeast cell. *Proc Natl Acad Sci USA* 104:16886–16891.
24. Klevecz RR, Bolen J, Forrest G, Murray DB (2004) A genomewide oscillation in transcription gates DNA replication and cell cycle. *Proc Natl Acad Sci USA* 101: 1200–1205.
25. Gracey AY, et al. (2008) Rhythms of gene expression in a fluctuating intertidal environment. *Curr Biol* 18:1501–1507.
26. Stöckel J, et al. (2008) Global transcriptomic analysis of Cyanothece 51142 reveals robust diurnal oscillation of central metabolic processes. *Proc Natl Acad Sci USA* 105: 6156–6161.
27. Takahashi JS, Hong HK, Ko CH, McDearmon EL (2008) The genetics of mammalian circadian order and disorder: implications for physiology and disease. *Nat Rev Genet* 9:764–775.
28. Picker A, Roellig D, Pourquié O, Oates AC, Brand M (2009) Tissue micromanipulation in zebrafish embryos. *Methods Mol Biol* 546:153–172.
29. Saeed AI, et al. (2006) TM4 microarray software suite. *Methods Enzymol* 411:134–193.